Focusing fluids in faults: Evidence from stable isotopic studies of dated clay-rich fault gouge of the Alberta Rockies

E. A. Lynch[1], D. Pană[2], and B. A. van der Pluijm[1]

[1]Department of Earth and Environmental Sciences, University of Michigan, 1100 N. University Ave, Ann Arbor, Michigan

[2]Alberta Geological Survey, Twin Atria Building, 4999-98 Avenue, Edmonton, Alberta T6B 2X3, Canada

Corresponding author: Erin Lynch (lynchea@umich.edu)

Key Points:

- Isotopic makeup of clay fault gouges document Late Mesozoic/Early Cenozoic deformational fluid regimes in the Canadian Cordillera thrust belt.
- Pervasive meteoric fluid was present during thrusting, with variable input from deeper metamorphic fluid sources.
- Fluid mixing was not dependent on spatial or temporal context in the fold-thrust belt.

Abstract

Isotopic studies of Canadian Rocky Mountain thrust faults preserve the timing and identity of orogenic fluids and their fault zone pathways. Using previously dated samples, we measure the O- and H-isotopic compositions of fault gouge. These nearly 100% neomineralized gouges and their associated damage zones act as primary orogenic fluid pathways. As such, they provide a specific and local look into the nature of the Late Jurassic to Early Eocene orogenic plumbing system in the Alberta Rockies. Considering clay polytype stability and regional temperature conditions, we obtain a range of geofluid isotopic compositions during Jurassic-Eocene thrust faulting: $\delta^{18}O_{fluid}$ ranged from ~ -3.3 to 9.2 ± 3.2‰; δD_{fluid} ranged from -119 to -46 ± 13‰ VSMOW. The range of O- and H-isotopic compositions reflects mixing of fluid sources, including the pervasive presence of surface-sourced fluids (up to ~90%). The interpreted prevalence of a surface fluid source in fault rocks is in agreement with regional isotopic trends previously observed in undated veins of fractured host rock. Our results confirm that thrust faults of the Alberta Rocky Mountains acted as major fluid-focusing conduits during orogenic activity. We further show that these faults incorporated both deeply-sourced and surface-sourced fluids into zones of enhanced and dynamic permeability, heterogeneously distributing fluids along fault planes across the fold-thrust belt, promoting the growth of fault-zone weakening clay minerals.

1. Introduction

Until the past few decades, the study of ancient, orogenic, shallow-crustal fluids has relied primarily on veins and fluid inclusions. These studies have identified surface (meteoric and basinal) fluids as a main component of vein-forming fluids, though deeply-sourced metamorphic and magmatic fluids were also considered (e.g. Evans & Battles, 1999; Bebout et al., 2001; Kirschner & Kennedy, 2001; Anastasio et al., 2004; Rygel et al., 2006; Travé et al., 2007; Cooley et al., 2011; Evans et al., 2012). Several studies have described the mixing of multiple crustal fluid sources in diverse crustal regimes and in numerous geographic locations (e.g. Nesbitt & Muehlenbacks, 1991; Travé et al., 2007; Cooley et al., 2011; Fitz-Diaz et al., 2014; Menzies et al., 2016). Clay mineral studies are a robust compliment to vein studies, since clays contain both structural H and O in their crystal lattice making them favorable for combined isotopic study. As with veins, isotopic studies of deformationally-mediated clay minerals, have invariably identified meteoric or surface-sourced fluids (including meteorically-derived basinal fluid) as a primary component of geofluids active during deformation (Fitz-Diaz et al., 2011, 2014; Boles et al., 2015, Haines et al., 2016; Lynch and van der Pluijm, 2016; Lynch et al., 2019). The crustal position of clay minerals in fault gouge, allows them to isotopically record the passage and/or presence of tectonic fluids as they mineralize, reducing friction along fault planes and promoting continued deformation.

Faults are generally interpreted as conduits for geofluid flow.The fault valve mechanism, proposed by Sibson (1992) has been cited as a method for transporting significant volumes of water through the brittle crust along structural discontinuities during episodes of fault activity. Both fault slip and fault-related deformation locally affects the permeability structure of the upper crust, providing far-reaching pathways of enhanced permeability surrounding active faults that exponentially decreases as distance from the fault plane increases, and that can vary by two to three orders of magnitude during cyclic deformation (Evans et al., 1997; Faulkner et al., 2010; Faulkner & Armitage, 2013). In this environment, other forces, such as burial pressure/temperature increases act as drivers controlling the geofluid flow vectors (Koons & Craw, 1991; Sibson, 1992). Notably, this fluid flow imparts chemical and mineral changes to the surrounding crustal rock, resulting in metasomatism and authigenic mineral growth. These processes leave behind an imprint of the geofluids involved during deformation, providing the opportunity to decipher the variable roles of orogenic fluid sources and their implications on the relative impacts of major fluid-driving forces.

The main sources of fluids in fold-thrust belts are, (1) the infiltration and subsequent expulsion of meteoric and basinal, surface-sourced fluids, and (2) the release and upward flow of deep, magmatic and metamorphic fluids (e.g. Walther & Wood, 1984; Fyfe & Kerrich, 1985; Bradbury & Woodwell, 1987; Ge & Garven, 1989; Koons & Craw, 1991; Dworkin, 1999; Menzies et al., 2014; Hüpers et al, 2017). Distinguishing between them can be done through targeted stable isotopic studies of fluid-grown minerals. The Canadian Rockies provides an ideal location to examine the contribution of deep vs surface fluids for several reasons. First, at high latitudes and high elevation, surface-derived meteoric waters are isotopically extremely light and, therefore, easily distinguished from other fluid sources by markedly negative hydrogen (δD) and oxygen ($\delta^{18}O$) isotopic signatures. Deep-sourced metamorphic and/or magmatic sources have considerably higher δ-values for hydrogen and oxygen.

However, the direct study of fault fluids has been difficult for several reasons, among them the lack of readily extractable and isolatable mineral phases in fault rock material. Advances in precision shallow fault-dating overcomes this particular hurdle, providing insight into the timing of fault activation though $^{40}Ar/^{39}Ar$-dating of secondary clay minerals separates that form during fluid flow in active fault zones (e.g., van der Pluijm et al., 2001). Building on dating of fault-grown mineral studies, this paper utilizes previously-dated clays from the Alberta Rocky Mountains (Pană and van der Pluijm, 2015) to determine the isotopic composition and source of fluids that were channeled through fault zones during episodic fault slip and regional deformation. Using fault gouge samples as fluid proxies is complementary to vein-based studies, as they provide independent insight into the absolute timing of fluid flow through Ar-dating, and isotopic studies utilize regional temperature constraints gained from fluid inclusion analysis. The application of paired oxygen and hydrogen isotopic analysis of dated clays provides a multi-dimensional picture of the role and location of fault rock fluids in major orogenic settings. This paper presents hydrogen and oxygen isotope data from the direct study of dated gouge, clarifying the relationship between regional deformation and localized faulting, associated fluid flow and fluid-driving forces in the southern Canadian Rockies Mountains.

2. Regional Geologic Context

Our study area is in the Alberta portion of the southern Canadian Rocky Mountain fold-and-thrust belt (RM-FTB), which is part of the Cordilleran Foreland belt of North America. Westerly from the Foreland belt, the southern Canada Cordillera is traditionally subdivided into the Omineca, Intermontane, Coast, and Insular morphogeological belts (e.g., Gabrielse et al., 1992) (Figure 1). The Foreland belt comprises strata of North American origin, the Omineca Belt is the region of overlap between ancestral North America and allochthonous rocks, whereas belts to the west include a collage accreted allochthonous and autochthonous terranes (e.g., Monger, 1984, 1989; Price, 1986, 1994). The upper-crustal tectonic elements (or allochthonous terranes) were juxtaposed over each other and over the western margin of the North American craton along a system of interleaved, northeast-and southwest-verging major thrust faults (Tempelman-Kluit, 1979; Monger et al., 1982; Struik, 1988).

Although the paleogeography and tectonic models of the southern Canadian Cordillera are somewhat controversial, it is widely accepted that Neoproterozoic rifting of Rodinia led to the onset of Windermere deposition and was followed by seafloor spreading and continental drift in the latest Neoproterozoic. By the earliest Cambrian a persistent continental shelf-slope system was established between ancient North America and the newly opened ocean, a distant ancestor of the present Pacific Ocean. The paleogeography of the ancient continental margin evolved from a passive margin until Middle Devonian to a mainly convergent plate margin until the present (e.g., Monger, 1984, 1989; Monger and Price, 2002).

Tectonic events did not markedly affect ancestral North American rocks in Canada until the Middle Jurassic. Events leading to Cordilleran mountain building started in Middle Jurassic time, as a result of breakup of Pangea and North American plate motion toward subduction zones at its western margin, followed by collisions with eastward and northeastward drifting island arcs on the proto-Pacific lithosphere (e.g., Monger et al., 1972, 1982; Monger, 1984, 1989; Gabrielse et al., 1992; Monger and Price, 2002). Between the Middle Jurassic and early Eocene, the Cordilleran realm was mainly under compression, accompanied at different times by sinistral and dextral transpression (e.g., Evenchick et al., 2007; Monger and Gibson, 2019).

The investigated RM-FTB formed as a thin-skinned accretionary wedge in a retroarc tectonic setting between the Middle Jurassic and early Eocene (Monger and Price, 2002; Pană and van der Pluijm, 2015). It is bounded to the east by the elusive eastern limit of Cordilleran deformation, and to the west by the Rocky Mountain trench. The detached and displaced supracrustal rocks comprise several broad tectono-stratigraphic assemblages, mostly of North American origin, deposited within the Western Canada sedimentary basin. The thick stack of east-vergent, generally downward- and eastward-younging thrust slices includes Proterozoic strata, locally overprinted by low- to medium-grade metamorphism, in the western parts of the RM-TFB, unmetamorphosed Paleozoic strata in the central and eastern parts, and Mesozoic to Cenozoic rocks in the frontal parts (Monger, 1989). The southernmost portion of the Canadian RM-FTB also includes strata of the Belt-Purcell Supergroup deposited in a controversial Mesoproterozoic tectonic setting (e.g., Ross and Villeneuve, 2003; Sears and Price, 2003).

3. Sample Location and Mineralogy

Fifteen (15) samples analyzed in this study were collected from the eastern, non-metamorphosed portion of the RM-FTB in Alberta, spanning the length of the belt from approximately 50 to 54 °N latitude (Figure 1, Table 1). Twelve (12) samples of fault gouge and one (1) footwall shale sample were previously dated using Ar geochronology (Pană & van der Pluijm, 2015); two (2) additional fault gouge ages were reported by van der Pluijm (2006). Using the combined illite ages from both studies, Pană and van der Pluijm (2015) identified four major pulses of contractional deformation between the Late Jurassic and Early Eocene, which preceded middle to late Eocene extensional collapse of the orogen. Authigenic illite shows that the growth of fault-related clay minerals occurred in the presence of ancient orogenic fluids, so their stable isotopic makeup reflects the stable isotopic composition of the deformational fluids. Though earlier work determined the polytypes of *illite* present in each gouge sample (required for Ar/Ar-dating), additional work was needed to fully characterize the clay mineralogy in order to extract the relevant isotopic signatures from authigenic illite.

The methods to process samples and characterize illitic materials are described in van der Pluijm et al. (2006) and Pană and van der Pluijm (2015). We completed additional clay mineral x-ray diffraction (XRD) characterization on the each of the four <2 μm size fractions through low-angle (2-40 °2θ) scanning of oriented mounts, which were prepared using the suspension method (Moore & Reynolds, 1997). We used a Cu-source Rigaku Ultima IV X-Ray Diffractometer equipped with a Ni foil k-beta filter, scanning at a speed of 1°/minute and a step size of 0.02 °2θ. Though illite was the dominant clay mineralogy for all samples, we also identified the presence of minor quartz, calcite, kaolinite, and chlorite in some of the samples (Figure 2). DP10-1 (Sample 7) also contained a trace amount of gypsum. Using the mineral reference intensities (MRI) method (Moore & Reynolds, 1997), we quantify the proportions of clay minerals present in each sample (Table 2).

4. Stable Isotopic Composition of Clay Gouge

4.1 Isotopic Measurement

Stable isotopic measurements of hydrogen and oxygen were completed at the Institute of Earth Surface Dynamics (IDYST) at the University of Lausanne (UNIL). Approximately 1.5–2mg of duplicate sample separates were encapsulated in silver foil packets and kept under vacuum for at least 12 hours prior to analysis. Samples were then quickly transferred to a helium-flushed zero-blank autosampler connected to a Thermo Finnigan Delta Plus XL thermochemical elemental analyzer (TC/EA). A helium carrier gas transferred the reduced hydrogen gas to the mass spectrometer, which measured the ratios of H_2 and DH gases, and the weight percent water for each sample. Results are reported using δ-notation relative to standard mean ocean water (SMOW) and are reproducible to ±3‰ across duplicate sample aliquots.

Prior to oxygen analyses, samples were loaded onto a platinum sample plate and heated in an oven at 150°C for at least 12 hours. Oxygen gas was isolated from silicate samples for isotopic measurements with laser fluorination (e.g., Sharp, 1990), using a vacuum of approximately 10^{-4} Pa prior to fluorination. Extracted oxygen gas was collected on a zeolite molecular sieve and transferred to a Finnigan MAT 253 Mass Spectrometer for measurement. As with hydrogen, results are reported using δ-notation relative to standard mean ocean water (SMOW) and are reproducible to ±0.2‰. We were unable to measure one sample (16: KKF-91-1A) for oxygen isotopic composition due to its reaction with F_2 gas at room temperature.

4.2 Hydrogen Isotopic Results

Two aliquots of each sample size fraction were measured for hydrogen isotopic composition. In nearly all cases, measurements are reproducible to ≤3‰, with the maximum error on duplicate measurements of 3.7‰ (sample 12: DP11-112MC) (Table 3).

A York-style bivariate linear regression analysis of hydrogen isotopic compositions and authigenic ($1M_d$) illite quantifications allows the extrapolation to 100% authigenic material and therefore, the determination of the hydrogen isotopic composition of deformation-related illite of the gouge (Table 4) (York, 1968; Boles et al., 2015; Lynch & van der Pluijm, 2016, Lynch et al., 2019). During preparation of one sample (sample 4:DP10-166D, Brule Thrust), hydrogen-rich organic material was concentrated by centrifugation into the fine fraction, which we discard to obtain a regression value of -136.5 ± 22.4‰ δD.

4.3 Oxygen Isotopic Results

Oxygen measurements were completed for the finest fraction of each sample. Unlike hydrogen, oxygen isotopic values are not affected by the presence of hydrocarbons that may concentrate into the finer fractions. Instead, oxygen isotopic values are affected by the presence of other rock-forming minerals, including silicates, oxides, and carbonates. Non-clay silicate minerals are absent in any of the finest fractions, except trace amounts of quartz and gypsum in sample 7 (DP10-1). Minor (<5 wt%) calcite was removed prior to oxygen isotopic analysis by reaction with 10% HCl. (Table 4). The variable presence of the $2M_1$, high-temperature detrital illite polymorph, which was seen in the fine fractions in concentrations up to 18±2% (Lewis Thrust, sample 18), with an average of 8±2%, is an irreducible source of error. Though we are unable to separate the authigenic from detrital illite in the finest fraction, we use the δO_{fine} values as representative of near-authigenic values. We find no systematic variation between the percentage of detrital illite and the δO_{fine} values.

5. Discussion

5.1 Fractionation Temperature Constraints

With constraints on fractionation temperature, the isotopic composition of mineralizing fluids is calculated from the isotopic composition of authigenic clay. Fractionation temperatures are constrained by the minimum formation temperature of 1Md illite, ~90°C (e.g., Haines & van der Pluijm, 2012). Maximum fractionation temperatures are obtained from mineralogic and other geologic evidence. A geothermal gradient of ~20-25°C/km has been estimated for the Canadian Rocky Mountain foreland fold-thrust belt region (e.g. England & Bustin, 1986; Hardebol et al., 2009; Osadetz et al., 2004). With a maximum thickness of ~8km for the deformed foreland wedge (Price, 1981; Pană & Elgr, 2013), this equates to temperatures less than 160-200°C. Additionally, Nesbitt & Muehlenbachs (1995) recorded fluid inclusion homogenization temperatures in calcite veins from the fold and thrust belt to be between 120° and 200°C. These observations, along with maximum temperature estimates from organic maturity indicators (Kalkreuth & McMechan, 1984; England & Bustin, 1986; Hardebol et al, 2009) and conodont alteration indices (Symons & Cioppa, 2002) characterize the thermal history of the fold-thrust belt and suggest that the viable temperature range during deformation was 100° - 200°C. Since many of the exhumed thrusts likely formed at shallower depths and, noting that the upper stability of low-temperature 1Md illite of ~180°C (Haines & van der Pluijm, 2012), we use an upper temperature of fault rock illite of 180^{o}C, reflecting absolute maximum thrusting and fault rock formation at 7-8 kilometers depth.

5.2 Characteristics and Identity of Mineralizing Fluid

We calculate the composition of the fluid isotopic values for a large temperature window to capture any uncertainty related to local variations in geothermal gradient and fluid-mediated heat exchange along the faults. Water composition was calculated using the fractionation equations of Sheppard and Gilg (1996) and Capuano (1992) for O and H respectively (Table 5, Figure 3). The range of results produced show a broad overlap between mineralizing fluids and Alberta Basin fluids (Hitchon & Friedman, 1969; Sheppard, 1986; Connolly et al., 1990), regardless of the temperature used for the fractionation calculation. On the higher end of the temperature range, fluids have slightly more positive $\delta^{18}O$ values and more negative δD values. This would imply more water-rock interaction and oxygen buffering (smaller water/rock ratio and/or longer fluid travel pathways through the fold thrust belt). However, the presences of very light hydrogen requires a high latitude or high elevation meteoric fluid as an original fluid source. One sample (sample 7: DP10-1) yields a fluid composition that very closely resembles the isotopic composition of seawater, suggesting that isolated pockets of connate seawater may have persisted locally prior to their expulsion along thrust faults. Several of the calculated isotopic fluid values overlap with the magmatic/metamorphic field, illustrating that though meteoric fluids are a major component in geofluids in many of the fault zones, deeper fluids likely also play a role in deformation. The range in isotopic values of mineralizing fluids show no systematic temporal or spatial pattern, indicating that fluid regimes did not vary with timing of orogenic pulse activity nor along orogenic trend (Figure 4).

5.3 Percentage Approximations of Fluid Mixing

To allow for discussion of fluid regimes, we simplify major crustal fluid sources into two bins: surface-sourced and deeply-sourced. Surface sources include meteoric fluids and meteorically-charged, relatively unevolved basinal fluids. Deep sources include magmatic, metamorphic, and highly evolved (high-temperature) basinal fluids. We assume that these ideal end-member fluids were homogeneous through time and space, and that the illitic clay material crystallized at constant temperatures, and under equilibrium fractionation conditions. This is a large oversimplification and is not intended to result in precise measurements or calculations. Instead we use this platform to spark a discussion around the heterogeneity that is observed in the samples through the lens of two ideal, end-member fluids. With this caveat, we present two fluids for consideration, which we refer to as “surface-sourced” and “and deeply-sourced” throughout the following discussion.

In order to define our surface-sourced end member, we applied a least squares regression to the data described in table 5 (excluding the outlying sample 7, which was the only sample containing gypsum, and whose fluid equivalent closely resembles SMOW) for both the maximum and minimum temperature constraints (Figure 5; Lynch and van der Pluijm, 2021). We extrapolate these regression lines to the intersection with the global meteoric water line ($\delta D = 8*\delta^{18}O+10‰$) (Sheppard, 1986). Fractionation at 90°C corresponds to a meteoric fluid with the isotopic signature of -13.5‰ $\delta^{18}O$ and -98 ‰ δD; fractionation at 180°C corresponds to a meteoric fluid with the isotopic signature of -21.0‰ $\delta^{18}O$ and -158‰ δD. These intersection points constrain the composition of the meteoric fluid input during fault activity, notably overalapping with penecontemporaneous surface fluids (Longstaffe & Ayalon, 1990; Bowen & Revenaugh, 2003; Chamberlain et al., 2012). The close correlation between the derived isotopic composition of surface fluids and the end-member meteoric fluid composition from fault gouge clays confirms that ancient meteoric fluids were a likely major fluid source in the evolving fold-thrust belt, variably mixing with heavier fluids (Figure 5). For our ideal surface-sourced fluid end member approximation, we define $\delta D_{surface}$ as -128‰ and $\delta^{18}O_{surface}$ as -15‰.

Previous studies emphasized the role of migrating, hot, metamorphic fluids during orogenesis (Nesbitt & Muehlenbachs, 1989; Machel & Cavell, 1999; Cooley et al., 2011). Because hydrogen isotopic signatures preserve the original fluid source—as they are not easily reset by water-rock interaction—we use fluid δD values from this study to estimate the relative proportions of end-member fluid input into fault zones. Based on the δD values of fluid inclusions and hydrous silicates in veins collected from greenschist facies in the fold-thrust belt—as high as -20‰—Nesbitt and Muehlenbachs (1989) suggested that most fluids involved in the Rocky Mountain thrusting originated from metamorphic devolatilization. Using this end-member δD values as representative of deeply-sourced water (δD_{deep} = -20‰) and the midpoint of our calculated MWL intersections as representative of meteoric water ($\delta D_{surface}$ = -128‰), we estimate the relative proportion of each fluid source. The average of our calculated fluid δD values (-78 ± 12‰, Table 5) would result from an approximately equal mixture of deeply-sourced and surface-sourced fluids (46%/54%), whereas the minimum fluid value (δD = -119 ± 13‰) is just over 90% surface derived, and the maximum (δD = -46 ± 13‰) from a 76%/24% deep/surface fluid mixture. The observed range of values indicates that mixing of fluid was not constant through time and space.

5.4 Implications for ancient fluid flow in the Canadian Rockies

The presence of both deeply-sourced and surface-sourced fluids in Rocky Mountain thrust faults allows us to explore the relative roles of fluid driving forces during deformation. The prevalance of surface fluids in the Canadian Rockies suggests that gravity—topographic head—is an important fluid driving force that promotes downward penetration of surface-sourced fluids across the mountain belts and foreland basins. This phenomenon has been proposed to explain meteoric isotopic signatures found in fluids of the Alpine fault of New Zealand, a major continental transform boundary (Koons and Craw, 1991; Menzies et al., 2014; 2016) and various Low-Angle Normal Faults of the US southwest (Haines et al., 2016). Despite the seemingly unfavorable stress regime, gravity-driven downward penetration of surface fluids through the upper crust is likely a dominant fluid driver in compressional belts as well.

At the same time that deforming fold-thrust belts allow gravity driven downward fluid penetration, they also present pathways for deeply-sourced, hot, high-pressure fluid to be expelled to the surface in response to buoyancy and compressional forces. During continued orogenesis, one might expect metamorphic fluid expulsion to peak during peak deformation, perhaps coinciding with the major deformation pulses described by Pană and van der Pluijm (2015). If this were the case, we would expect the earliest fault fluids to be dominated by surface sources, peak deformation to be accompanied by increased metamorphic/magmatic fluid release, and late stage orogenesis to be again dominated by surface-fluids. Looking at figure 4A, we are tempted to conclude that this is the case for $\delta^{18}O$—oldest and youngest fluids seem to be more negative (similar to surface-sourced fluids), whereas those in the middle of the age range seem less negative (similar to metamorphic fluids). However, figure 4B does not show the same pattern for δD, and considering our uncertainties the data does not permit us to take such a bold stand. Interestingly, Nesbitt and Muehlenbachs (1994) did observe a predominance of likely meteoric fluids in their study of postorogenic veins, implying that deep-sourced fluids were not available for mineralization while deformation had nearly ceased. This could also have been due to the fact that the sampled veins were not long-lived conduits for flow, as the thrust faults likely were.

Regardless, though we find isotopic evidence for the involvement of deeply-sourced fluids in the RM-FTB, we do not see any clear pattern in the isotopic composition of these fluids that can be easily attributed to either systematically changing fluid inputs or different source compositions through time or during orogenic pulses (Figure 4). Instead, the relative contribution of these deep fluids and surface fluids appears to be heterogeneous through time and across the mountain belt. This suggests one of two things: that local heterogeneities in stress regime and rock fracturing may be a driving factor promoting local to regional scale fluid infiltration to fault-depths, and/or that deeply sourced fluids are not released en masse during progressive deformation. As the two (or more) fluids migrate and mingle, they find crustal weaknesses in the thrust faults and promote new mineral growth therein, including friction-reducing clays. A more thorough sampling campaign, one that combines fault gouge studies with vein studies from the same outcrops, and places them in temperature-depth context on a palinspastically restored cross-section may, in the future, be able to further eliminate uncertainties in this study and continue to unlock the fluid mixing puzzle in fold-thrust belts.

6. Conclusions

Newly formed clays in fault rock that are found along major thrust faults in the Alberta Rockies allow us to determine the ancient sources and pathways of orogenic fluids during shallow crustal deformation. We examined fault fluids through isotopic analysis of secondarily-formed, fault-grown, dated clays in fault gouge and explored the degree of fluid mixing in fault zones. Vein-based studies in older host rock have variably identified metaphorphic fluid as a significant contributor during compressional deformation (Cooley et al., 2011; Nesbitt and Muehlenbachs, 1991, 1994; Machel and Cavell, 1999), whereas our study of fault gouge shows that surface-sourced fluids often dominate and that they are efficiently channeled along fault block interfaces. Moreover, our study constrains the degree of mixing of fluid reservoirs and their relative volumetric contributions.

Rather than painting a simple picture of single fluid activity, or homogenous fluid migration across or along faults, our results show that fluid systems in the RM-FTB are multi-dimensional and complex. Variable mixing of fluids implies that the fluid regime in the fold-thrust belt was an open system, allowing the introduction, movement, and mixing of different fluids throughout ongoing deformation, focused along active thrust faults toward the front and foreland of the mountain range.

Acknowledgments

This project was supported by a Rackham Graduate School Predoctoral Fellowship to Lynch. Field and analytical support was provided by AER/Alberta Geological Survey. Support for clay research at the University of Michigan was provided by the National Science Foundation (most recently EAR-1629805). We thank Torsten Vennemann and Benita Putlitz for invaluable help and guidance in the stable isotope laboratory at UNIL. Thanks are also extended to Randy Williams, Mark Evans, and two anonymous reviewers, whose questions and contributions greatly improved and focused this paper.

Figure Captions

Figure 1. Geologic map and cross section after Pană and van der Pluijm, 2015. The locations of samples collected from the Canadian Cordillera fold-thrust belt in Alberta are shown on the map and positioned relatively on the cross section. Italicized thrust names listed on the cross section do not intersect the section. Sample A (a footwall shale sample) shares the same location (within 300 m) as Sample 9. Samples 13-15 and 17 from Pană and van der Pluijm, 2015 were not available for use in this study.

Figure 2. Two representative series of oriented XRD patterns. In both diagrams, the coarsest fraction is on the top, the finest fraction on the bottom. The left patterns (DP10-2) are representative of the several samples whose clay mineralogy contain only illite. The right patterns (DP11-107) are more representative of samples that have two clay minerals present, in this case, illite and chlorite. Both samples also indicate the presence of quartz, particularly in the coarser fractions (peaks at 20.8 and 26.5°2θ). The right sample also shows evidence of calcite, present in the two finer fractions (peak at 29.4 °2θ).

Figure 3. Plot of isotopic composition of samples, mineralizing fluids, and major crustal fluid reservoirs. Each calculated fluid composition is shown as a blue-red (left-right) colored bar representing the range of possible δD and $\delta^{18}O$ values over the 90° to 180°C fractionation temperature range. Each fluid bar is labeled with a number in a small white circle, corresponding

to sample numbers which were reported in table 5. Major fluid reservoirs shown include metamorphic fluids (grey box), magmatic fluids (black box), Alberta/West Canada sedimentary basin fluids (blue shaded region), meteoric water (dark grey line) and standard mean ocean water (SMOW, black circle) (Hitchon and Friedman, 1969; Sheppard, 1986; Connolley et al., 1990). Calculated fluid values largely overlap with basin fluids and partly with metamorphic/magmatic fluids. One fluid value corresponds with ocean water isotopic composition.

Figure 4. Series of cross-plots examining fluid isotopic signatures through time and with respect to position in the RM-FTB. A and B show the relation of timing of in-sequence fault slip to $\delta^{18}O$ and δD of fault fluids. Fault ages from Pană and van der Pluijm (2015) and van der Pluijm et al. (2006). Plots C and D show isotopic composition with respect to latitude. Plots E and F compare isotopic composition to their relative positions in the FTB. The latter is expressed as a fractional distance across the belt, with 0 corresponding to the Southern Rocky Mountain Trench (SMRT) and 1 to the Approximate Limit of Cordilleraian Deformation (LCD) (both shown in Figure 1). The width is the measured distance from the SMRT to the LCD, perpendicular to the strike of the belt through each sample location. Error is estimated to be ± 0.1. Considering error and uncertainty, there is no correlation between any of the variables explored and fluid isotopic composition.

Figure 5 Schematic representation of the isotopic composition of fluids in the Alberta fold-thrust belt. Clay measurements from this study are encompassed by the white outlined region; the calculated mineralizing fluid compositions by the blue outlined region. The results of our least-squares regression for fractionation temperature range define the window of likely meteoric fluid compositions between where the dotted regression lines intersect the global Meteoric Water Line. This window overlaps with the δD and $\delta^{18}O$ values of modern Canadian Cordillera meteoric fluid (Longstaffe & Ayalon, 1990; Bowen & Revenaugh, 2003), which is shown as a black oval, and considered to be one of the end-member mixing fluids. It is likely that during orogenic activity, local meteoric waters would have been less negative than they are today, due both to the lower elevation and lower latitude during the early stages of mountain building. The stippled grey box shows the region of syn- to postorogenic fluids (Nesbitt & Muehlenbachs, 1994) interpreted from fluids inclusions in dolomite veins, which have a slight overlap with clay mineralizing fluids.

Samples and Data

Datasets for this research are additionally available via "Deep Blue," the University of Michigan's data repository: Lynch et al. (2021), [CC0 1.0, doi: 10.7302/6emc-9f49]

References

Anastasio, D.J., Bebout, G.E., & Holl, J.E. (2004), Extra-basinal fluid infiltration, mass transfer, and volume strain during folding: Insights from the Idaho-Montana thrust belt. *American Journal of Science*, *304*(4), 333–369, doi: 10.2475/ajs.304.4.333.

Bebout, G.E., Anastasio, D.J., & Holl, J.E. (2001), Synorogenic crustal fluid infiltration in the Idaho-Montana Thrust Belt. *Geophysical Research Letters*, *28*(22), 4295–4298, doi: 10.1029/2001GL013711.

Boles, A., van der Pluijm, B., Mulch, A., Mutlu, H., Uysal, T., & Warr, L. (2015), Hydrogen and ^{40}Ar/^{39}Ar isotope evidence for multiple and protracted paleofluid flow events within the long-lived North Anatolian Keirogen (Turkey): *Geochemistry, Geophsysics, Geosystems*, *16*(6), 1975-1987, doi: 10.1002/2015GC005810.

Bowen, G.J., & Revenaugh, J. (2003), Interpolating the isotopic composition of modern meteoric precipitation. *Water Resources Research*, *39*(10), doi: 10.1029/2003WR002086.

Bradbury, H.J & Woodwell, G.R. (1987), Ancient fluid flow within foreland terrains. *Geological Society, London, Special Publications*, *34*, p. 87–102, doi: 10.1144/GSL.SP.1987.034.01.07.

Capuano, R. (1992), The temperature dependence of hydrogen isotope fractionation between clay minerals and water: Evidence from a geopressured system. *Geochimica et Cosmochimica Acta*, *56*, 2547-2554, doi: 10.1016/0016-7037(92)90208-Z.

Chamberlain, C.P., Mix, H.T., Mulch, A., Hren, M.T., Kent-Corson, M.L., Davis, S.J., Horton, T.W., & Graham, S.A. (2012), The Cenozoic climatic and topographic evolution of the western North American Cordillera. *American Journal of Science, 312*(2), 213–262, doi: 10.2475/02.2012.05.

Cooley, M.A., Price, R.A., Kyser, T.K., & Dixon, J.M. (2011), Stable-isotope geochemistry of syntectonic veins in Paleozoic carbonate rocks in the Livingstone Range anticlinorium and their significance to the thermal and fluid evolution of the southern Canadian foreland thrust and fold belt. *AAPG Bulletin*, *95*(11), 1851–1882, doi: 10.1306/01271107098.

Dworkin, S.I. (1999), Geochemical constraints on the origin of thrust fault fluids. *Geophysical Research Letters*, *26*(24), 3665–3668, doi: 10.1029/1999GL008377.

England, T.D.J., & Bustin, R.M. (1986), Effect of thrust faulting on organic maturation in the southeastern Canadian Cordillera. *Organic Geochemistry*, *10*(1-3), 609–616, doi: 10.1016/0146-6380(86)90057-4.

Evans, J.P., Forster, C.B., and Goddard, J.V. (1997), Permeability of fault-related rocks, and implications for hydraulic structure of fault zones. *Journal of Structural Geology*, *19* (11), 1393-1404, doi: 10.1016/S0191-8141(97)00057-6.

Evans, M.A., & Battles, D.A. (1999), Fluid inclusion and stable isotope analyses of veins from the central Appalachian Valley and Ridge province: Implications for regional synorogenic hydrologic structure and fluid migration. *Geological Society of America Bulletin*, *111*(12), 1841–1860, doi: 10.1130/0016-7606(1999)111<1841:FIASIA>2.3.CO;2.

Evans, M.A., Bebout, G.E., & Brown, C.H. (2012), Changing fluid conditions during folding: An example from the central Appalachians. *Tectonophysics*, *576-577*, 99–115, doi: 10.1016/j.tecto.2012.03.002.

Evenchick, C.A., McMechan, M.E., McNicoll, V.J., and Carr, S.D. (2007), A synthesis of the Jurassic-Cretaceous tectonic evolution of the central and southeastern Canadian Cordillera: Exploring links across the orogen. In L.W. Sears, T.A. Harms, and C.A Evenchick, (Eds.), *Whence the Mountains? Inquiries into the Evolution of an Orogenic System: A Volume in Honor of Raymore A. Price: GSA Special Paper*, (no. 443, p. 117-145), doi: 10.1130/2007.2433(06).

Faulkner, D.R., & Armitage, P.J. (2013), The effect of tectonic environment on permeability development around faults and in brittle crust. *Earth and Planetary Science Letters*, *375*, 71-77, doi: 10.1016/j.epsl.2013.05.006.

Faulkner, D.R, Jackson, C.A.L, Lunn, R.J., Schlische, R.W., Shipton, Z.K., Wibberley, C.A.J., & Withjack, M.O. (2010), A review or recent developments concerning the structure, mechanics and fluid flow properties of fault zones. *Journal of Structural Geology*, *32*, 1557–1575, doi: 10.1016/j.jsg.2010.06.009.

Fitz-Diaz, E., Camprubí, A., Cienfuegos-Alvarado, E., Morales-Puente, P., Schleicher, A.M., & van der Pluijm, B.A. (2014), Newly-formed illite preserves fluid sources during folding of shale and limestone rocks; an example from the Mexican Fold-Thrust Belt. *Earth and Planetary Science Letters*, *391*, 263–273, doi: 10.1016/j.epsl.2013.12.025.

Fyfe, W.S., & Kerrich, R. (1985), Fluids and thrusting. *Chemical Geology*, *49*(1-3), 353–362, doi: 10.1016/0009-2541(85)90167-6.

Gabrielse, H., Monger, J.W.H., Wheeler, J.O., and Yorath, C.J. (1992), Morphogeological belts, tectonic assem- blages, and terranes: Chapter 2, Part A. In H. Gabrielse and C.J Yorath, (Eds.), *Geology of the Cordilleran Orogen in Canada. Geological Survey of Canada, Geology of Canada*, *4* (also Geological Society of America, The Geology of North America, v. G-2), 15–28, doi: 10.4095/134073.

Ge, S & Garven, G. (1989), Tectonically Induced Transient Groundwater Flow in Foreland Basin. *Geophysical Monograph Series*, *14*(3), 145-157, doi: 10.1029/GM048p0145.

Haines, S., & van der Pluijm, B. (2012), Patterns of mineral transformations in clay gouge, with examples from low-angle normal fault rocks in the western USA. J*ournal of Structural Geology*, *43*, 2 – 32, doi: 10.1016/j.jsg.2012.05.004.

Hardebol, N.J., Callot, J.P., Bertotti, G., & Faure, J.L. (2009), Burial and temperature evolution in thrust belt systems: Sedimentary and thrust sheet loading in the SE Canadian Cordillera. *Tectonics*, *28*(3), doi: 10.1029/2008TC002335.

Hüpers, A., Torres, M.E., Owari, S., McNeill, L.C., Dugan, B., Henstock, T.J., Milliken, K.L., Petronotis, K.E., et al., (2017), Release of mineral-bound water prior to subduction tied to shallow seismogenic slip off Sumatra. *Science*, *356*(6340), 841–844, doi: 10.1126/science.aal3429.

Kalkreuth, W., & McMechan, M.E. (1984), Regional pattern of thermal maturation as determined from coal-rank studies, Rocky Mountain Foothills and Front Ranges north of

Grande Cache, Alberta - implications for petroleum exploration. *Bulletin of Canadian Petroleum Geology*, *32*(3), 249–271, doi: 10.35767/gscpgbull.32.3.249.

Kirschner, D.L., & Kennedy, L.A. (2001), Limited syntectonic fluid flow in carbonate-hosted thrust faults of the Front Ranges, Canadian Rockies, inferred from stable isotope data and structures. *Journal of Geophysical Research*, *106*(B5), 8827-8840, doi: 10.1029/2000JB900414.

Koons, P.O., & Craw, D. (1991), Evolution of Fluid Driving Forces and Composition Within Collisional Orogens. *Geophysical Research Letters*, *18*(5), 935–938, doi: 10.1029/91GL00910.

Longstaffe, F.J., & Ayalon, A. (1990), Hydrogen-isotope geochemistry of diagenetic clay minerals from Cretaceous sandstones, Alberta, Canada: evidence for exchange. *Applied Geochemistry*, *5*(5), 657–668, doi: 10.1016/0883-2927(90)90063-B.

Lynch, E.A., & van der Pluijm, B.A. (2016), Meteoric fluid infiltration in the Argentine Precordillera fold-and-thrust belt: Evidence from H isotopic studies of neoformed clay minerals. *Lithosphere*, *9*(1), L568.1–12, doi: 10.1130/L568.1.

Lynch, E.A., Mulch, A., Yonkee, A., & van der Pluijm, B.A. (2019), Surface fluids in the evolving Sevier fold-thrust belt of ID-WY indicated by hydrogen isotopes in dated, authigenic clay minerals. *Earth and Planetary Science Letters*, *513*, 29-39, doi: 10.1016/j.epsl.2019.02.003.

Lynch, E., van der Pluijm, B. (2021). *Canadian Cordillera Fault Gouge XRD and isotopes* [Data set], University of Michigan - Deep Blue Data. https://doi.org/10.7302/6emc-9f49.

Machel, H.G., & Cavell, P.A. (1999), Low-flux, tectonically-induced squeegee fluid flow ("hot flash") into the Rocky Mountain Foreland Basin. *Bulletin of Canadian Petroleum Geology*, *47*(4), 510–533, doi: 10.35767/gscpgbull.47.4.510.

Menzies, C., Teagle, D., Craw, D., Cox, S., Boyce, A., Barrie, C., & Roberts, S. (2014), Incursion of meteoric waters into the ductile regime in an active orogen. *Earth and Planetary Science Letters*, *399*, 1-13, doi: 10.1016/j.epsl.2014.04.046.

Menzies, C.D., Teagle, D.A.H., Niedermann, S., Cox, S.C., Craw, D., Zimmer, M., Cooper, M.J., & Erzinger, J. (2016), The fluid budget of a continental plate boundary fault: Quantification from the Alpine Fault, New Zealand. *Earth and Planetary Science Letters*, *445*, 125–135, doi: 10.1016/j.epsl.2016.03.046.

Moore, D.M., & Reynolds Jr., R.C. (1997), *X-Ray Diffraction and the Identification and Analysis of Clay Minerals*, New York, NY: Oxford University Press.

Monger, J.W.H. (1984), Cordilleran tectonics: A Canadian perspective. *Bulletin of the Geological Society of France*, *XXXVI-7*, 255–278, doi: 10.2113/gssgfbull.S7-XXVI.2.255.

Monger, J.W.H. (1989), Overview of Cordilleran geology; Chapter 2. In Ricketts, B.D., (Ed.), *Western Canada Sedimentary Basin: A Case History*. Calgary, Canadian Society of Petroleum Geologists, 9–32.

Monger, J.W.H., Gabrielse, H., and Souther, J.G. (1972), Evolution of the Canadian Cordillera: A plate-tectonic model. *American Journal of Science, 272*, 577–602, doi:10.2475/ajs.272.7.577.

Monger, J.W.H., Price, R.A., and Tempelman-Kluit, D.J. (1982), Tectonic accretion and the origin of two major metamorphic and plutonic welts in the Canadian Cordillera. *Geology*, *10*, 70–75, doi:10.1130/0091 -7613(1982)10<70:TA ATOO>2.0.CO;2.

Monger, J.W.H., and Price, R.A. (2002), The Canadian Cordillera: Geology and tectonic evolution. *Canadian Society of Exploration Geophysicists*, *Recorder*, 17–36.

Monger, J.W.H, and Gibson, H.D. (2019), Mesozoic-Cenozoic deformation in the Canadian Cordillera: The record of a "Continental Bulldozer"? *Tectonophysics, 757*, 153-169, doi: 10.1016/j.tecto.2018.12.023.

Nesbitt, B.E., & Muehlenbachs, K. (1989), Geology, Geochemistry, and Genesis of Mesothermal Lode Gold Deposits of the Canadian Cordillera: Evidence for Ore Formation from Evolved Meteoric Water. In R. R. Keays, W. Ramsay, & D. I. Groves, (Eds.), *Economic Geology Monograph Series*, *6*, 553–563, doi: doi.org/10.5382/Mono.06.42.

Nesbitt, B.E., & Muehlenbachs, K. (1991), Stable isotopic constraints on the nature of the syntectonic fluid regime of the Canadian Cordillera. *Geophysical Research Letters*, *18*(5), 963-1066, doi: 10.1029/91GL00914.

Nesbitt, B.E., & Muehlenbachs, K. (1994), Paleohydrogeology of the Canadian Rockies and origins of brines, Pb- Zn deposits and dolomitization in the Western Canada Sedimentary Basin. *Geology*, *22*(3), 243-246, doi: 10.1130/0091-7613(1994)022<0243:POTCRA>2.3.CO;2.

Nesbitt, B.E., & Muehlenbachs, K. (1995), Geochemical studies of the origins and effects of synorogenic crustal fluids in the southern Omineca Belt of British Colombia, Canada. *GSA Bulletin*, *107*, 1033-1050, doi: 10.1130/0016-7606(1995)107<1033:GSOTOA>2.3.CO;2.

Osadetz, K. G., B. P. Kohn, S. Feinstein, & R. A. Price (2004), Foreland belt thermal history using apatite fission-track thermochronology: Implications for Lewis thrust and Flathead fault in the southern Canadian Cordilleran petroleum province. In R. Swennen, F. Roure, and J. W. Granath, (Eds.), *Deformation, fluid flow, and reservoir appraisal in foreland fold and thrust belts: AAPG Hedberg Series*, (no. 1, p. 21–48), doi: 10.1306/1025684H13111.

Pană, D.I., & Elgr, R. (2013), Geological Map of the Alberta Rocky Mountains and Foothills (NTS 82G, 82H, 82J, 82O, 82N, 83B, 83C, 83D, 83F, 83E, and 83L). (Map 560, scale 1:500 000). Energy Resources Conservation Board (ERCB)/Alberta Geological Survey (AGS), Alberta, Canada, http:// www .ags .gov .ab .ca /publications /MAP /PDF /MAP 560 .PDF.

Pană, D.I., & van der Pluijm, B.A. (2015), Orogenic pulses in the Alberta Rocky Mountains: Radiometric dating of major faults and comparison with the regional tectono-stratigraphic record. *Geological Society of America Bulletin*, *127*(3-4), 480–502, doi: 10.1130/B31069.1.

Price, R.A. (1981), The Cordilleran foreland thrust and fold belt in the southern Canadian Rocky Mountains. *Geological Society, London, Special Publications*, *9*(1), 427-448, doi: 10.1144/gsl.sp.1981.009.01.39.

Price, R.A. (1986), The southeastern Canadian Cordillera: Thrust faulting, tectonic wedging, and delamination of the lithosphere. *Journal of Structural Geology, 8*, 239–254, doi:10.1016/0191-8141(86)90046-5.

Price, R.A. (1994), Cordilleran tectonics and the evolution of the Western Canada sedimentary basin. In G. Mossop and I. Shetsen, (Compilers), *Geological Atlas of the Western Canada Sedimentary Basin. Calgary, Canada, Canadian Society of Petroleum Geologists and Alberta Research Council*, 13–24.

Ross, G.M., and Villeneuve, M. (2003), Provenance of the Mesoproterozoic (1.45 Ga) Belt basin (western North America): Another piece in the pre-Rodinia paleogeographic puzzle. *Geological Society of America Bulletin, 115*(10), 1191–1217, doi:10.1130/B25209.1

Rygel, A.C., Anastasio, D.J., & Bebout, G.E. (2006), Syntectonic infiltration by meteoric waters along the Sevier thrust front, southwest Montana, *Geofluids*, *6*(4), 288–301, doi: 10.1111/j.1468-8123.2006.00146.x.

Sears, J.W., and Price, R.A., (2003), Tightening the Siberian connection to western Laurentia. *Geological Society of America Bulletin*, *115*, 227-246, doi: 10.1130/B25229.1.

Sharp, Z.D. (1990), A laser-based microanalytical method for the in situ determination of oxygen isotope ratios of silicates and oxides. *Geochimica et Cosmochimica Acta*, *54*(5), 1353–1357, doi: 10.1016/0016-7037(90)90160-M.

Sheppard, S.M.F. (1986), Characterization and isotopic variations in natural waters: *Reviews in Mineralogy and Geochemistry*, *16*(1), 165–183.

Sheppard, S., & Gilg, H. (1996), Stable isotope geochemistry of clay minerals. *Clay Minerals*, *31*(1), 1-24, doi: 10.1180/claymin.1996.031.1.01.

Struik, L.C. (1988) Crustal evolution of the eastern Canadian Cordillera. *Tectonics, 7*, 727–747, doi:10.1029 /TC007i004p00727.

Symons, D.T.A., & Cioppa, M.T. (2002), Conodont CAI and magnetic mineral unblocking temperatures: Implications for the Western Canada Sedimentary Basin. *Physics and Chemistry of the Earth*, *27*(25-31), 1189–1193, doi: 10.1016/S1474-7065(02)00129-8.

Tempelman-Kluit, D.J. (1979) Transported Cataclasite, Ophiolite, and Granodiorite in Yukon: Evidence of Arc-Continent Collision. *Geological Survey of Canada Paper 79–14*, 27 p.

Travé, A., Labaume, P., & Verges, J. (2007), Fluid systems in foreland fold-and-thrust belts: An overview from the Southern Pyrenees. In O. Lacombe, J. Lave, F. Roure, J. Verges (Eds.), *Thrust belts and foreland basins: from fold kinematics to hydrocarbon systems*. (pp. 99-114). Springer, Berlin, Heidelberg. doi: 10.1007/978-3-540-69426-7_5.

van der Pluijm, B.A., Hall, C.M., Vrolijk, P., Pevear, D.R., and Covey, M.C. (2001), The dating of shallow faults in the Earth's crust: *Nature*, *412*, 172-174, doi: 10.1038/35084053.

van der Pluijm, B.A., Vrolijk, P., Pevear, D.R., Hall, C.M., & Solum, J.G. (2006), Fault dating in the Canadian Rocky Mountains: Evidence for late Cretaceous and early Eocene orogenic pulses. *Geology*, *34*(10), 837–840, doi: 10.1130/G22610.1.

Walther, J.V., & Wood, B.J. (1984), Rate and mechanism in prograde metamorphism. *Contributions to Mineralogy and Petrology*, *88*(3), 246–259, doi: 10.1007/BF00380169.

York, D. (1968), Least squares fitting of a straight line with correlated errors. *Earth and Planetary Science Letters*, 5, 320-324.

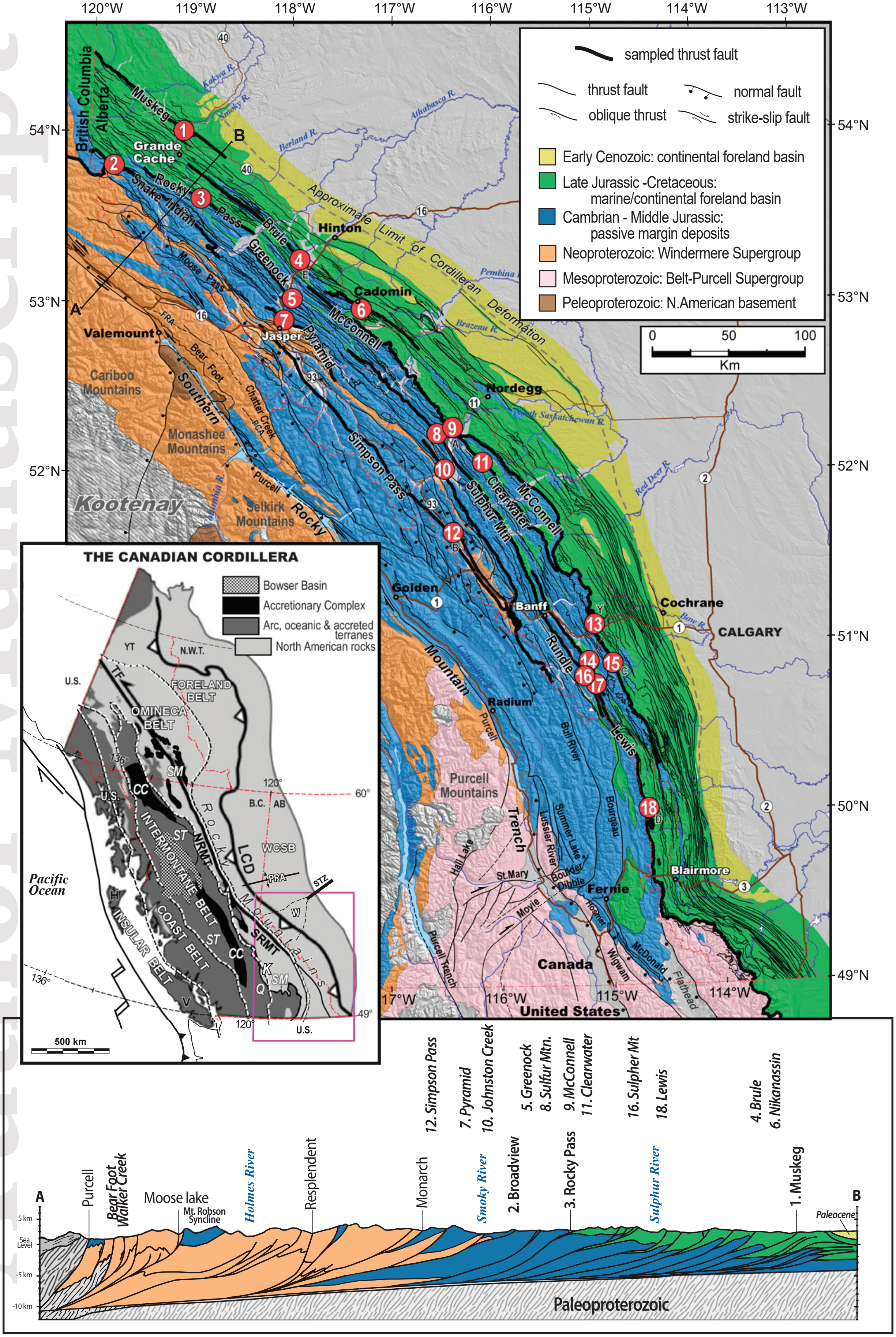

120°W
119°W
118°W
117°W
116°W
115°W
114°W
113°W
54°N
53°N
52°N
51°N
50°N
49°N
sampled thrust fault
thrust fault
normal fault
oblique thrust
strike-slip fault
Early Cenozoic: continental foreland basin
Late Jurassic -Cretaceous: marine/continental foreland basin
Cambrian - Middle Jurassic: passive margin deposits
Neoproterozoic: Windermere Supergroup
Mesoproterozoic: Belt-Purcell Supergroup
Paleoproterozoic: N.American basement
0
50
100
Km
British Columbia
Alberta
Muskeg
Grande Cache
Rocky Pass
Snake Indian
Brule
Greenock
Hinton
Cadomin
McConnell
Pyramid
Jasper
Valemount
Moose Pass
Bear Foot
Cariboo Mountains
Southern
Monashee Mountains
Chatter Creek
Purcell
Selkirk Mountains
Rocky
Kootenay
Approximate Limit of Cordilleran Deformation
Nordegg
Simpson Pass
Clearwater
Sulphur Mtn
Golden
Banff
Cochrane
CALGARY
Rundle
Mountain
Radium
Purcell Mountains
Trench
Bull River
Lewis
Bourgeau
Summer Lake
Lussier River
Hall Lake
St.Mary
Boulder
Dibble
Moyie
Fernie
Blairmore
Purcell Trench
Canada
United States
Wigwam
McDonald
Flathead
THE CANADIAN CORDILLERA
Bowser Basin
Accretionary Complex
Arc, oceanic & accreted terranes
North American rocks
YT
N.W.T.
U.S.
FORELAND BELT
OMINECA BELT
SM
CC
ST
INTERMONTANE BELT
NRMT
Rocky Mountains
LCD
WCSB
PRA
STZ
B.C.
AB
60°
120°
136°
Pacific Ocean
INSULAR BELT
COAST BELT
SRMT
K
Q
V
W
49°
500 km
12. Simpson Pass
7. Pyramid
10. Johnston Creek
5. Greenock
8. Sulfur Mtn.
9. McConnell
11. Clearwater
16. Sulpher Mt
18. Lewis
4. Brule
6. Nikanassin
A
B
Purcell
Bear Foot
Walker Creek
Moose lake
Mt. Robson Syncline
Holmes River
Resplendent
Monarch
Smoky River
2. Broadview
3. Rocky Pass
Sulphur River
1. Muskeg
Paleocene
5 km
Sea Level
-5 km
-10 km
Paleoproterozoic

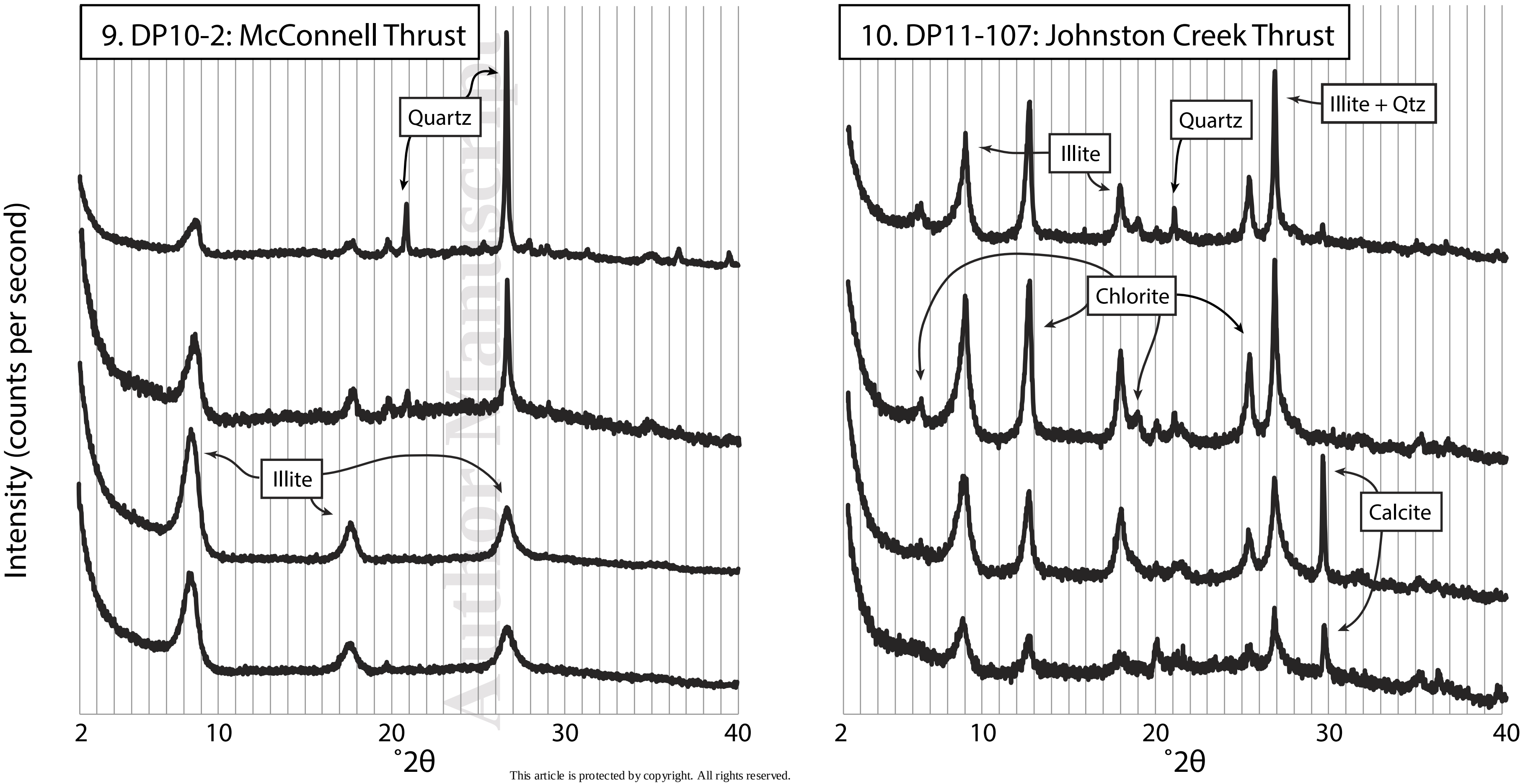
9. DP10-2: McConnell Thrust
Quartz
Illite
Intensity (counts per second)
2
10
20
30
40
°2θ
10. DP11-107: Johnston Creek Thrust
Illite + Qtz
Quartz
Illite
Chlorite
Calcite
2
10
20
30
40
°2θ

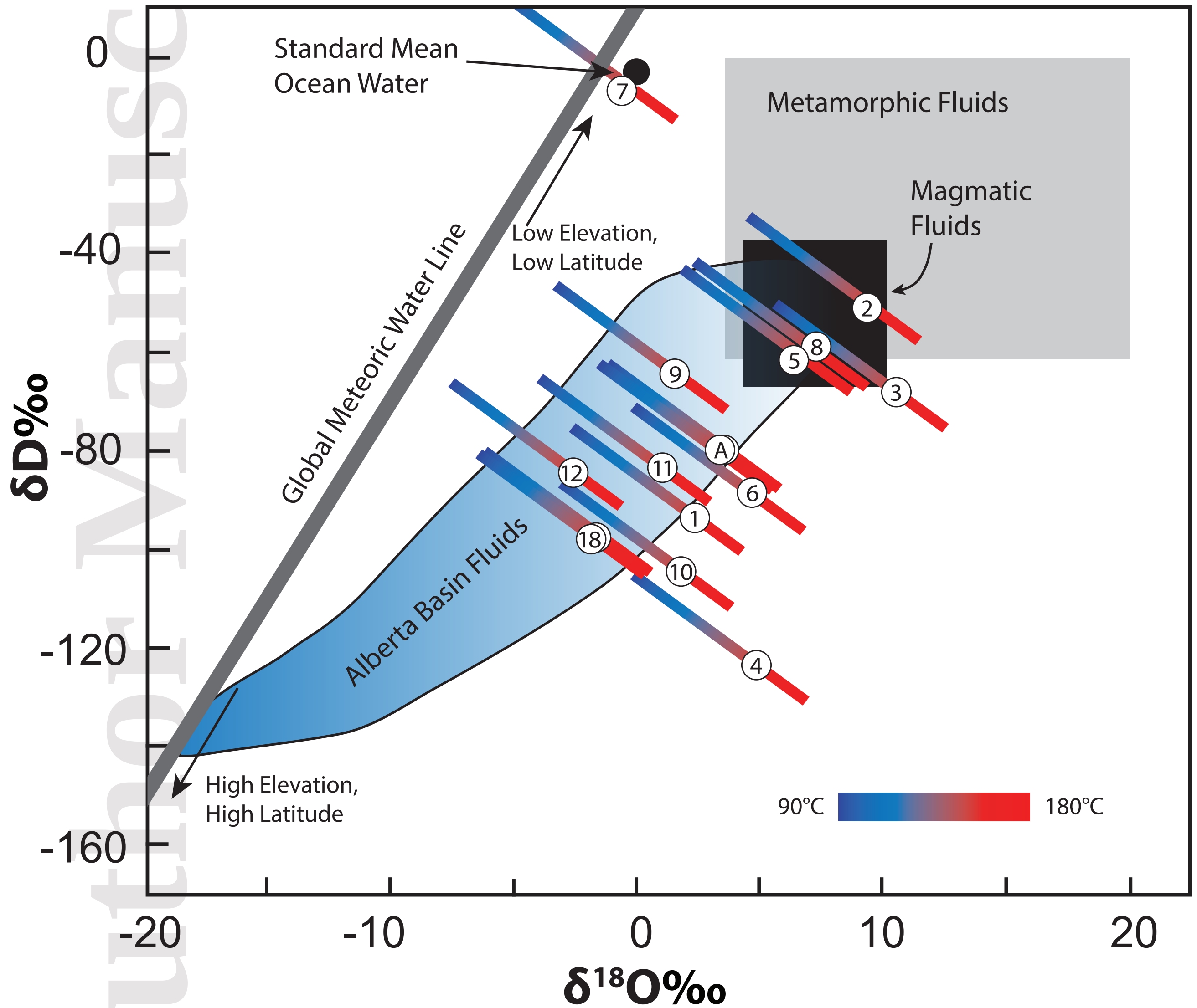

Standard Mean
Ocean Water
Metamorphic Fluids
Magmatic
Fluids
Low Elevation,
Low Latitude
Global Meteoric Water Line
Alberta Basin Fluids
High Elevation,
High Latitude
90°C
180°C
0
-40
-80
-120
-160
-20
-10
0
10
20
δD‰
δ18O‰
7
2
8
5
3
9
A
11
6
12
1
18
10
4

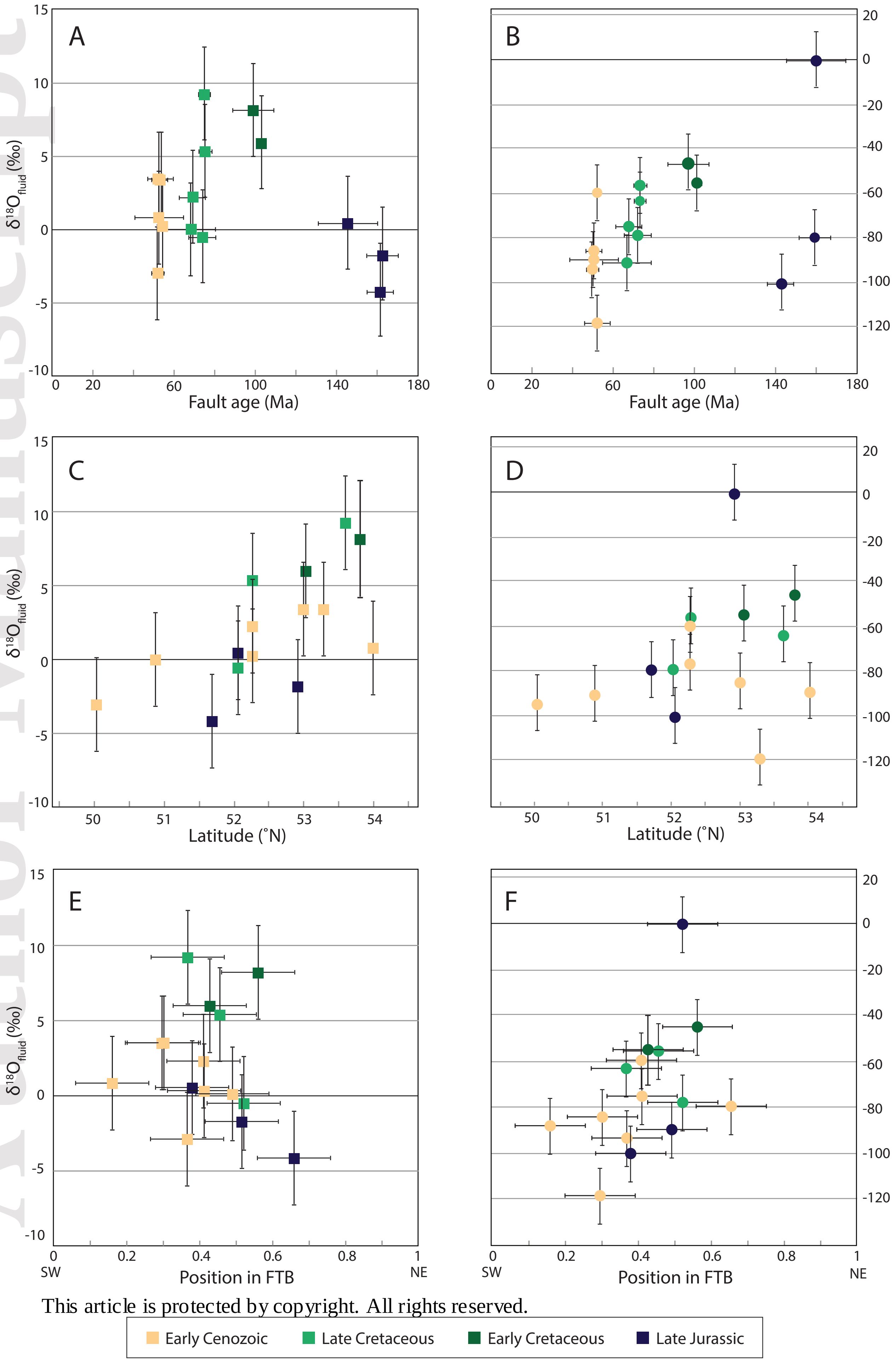

A
B
C
D
E
F
δ18O fluid (‰)
δD fluid (‰)
Fault age (Ma)
Latitude (˚N)
Position in FTB
SW
NE
Early Cenozoic
Late Cretaceous
Early Cretaceous
Late Jurassic

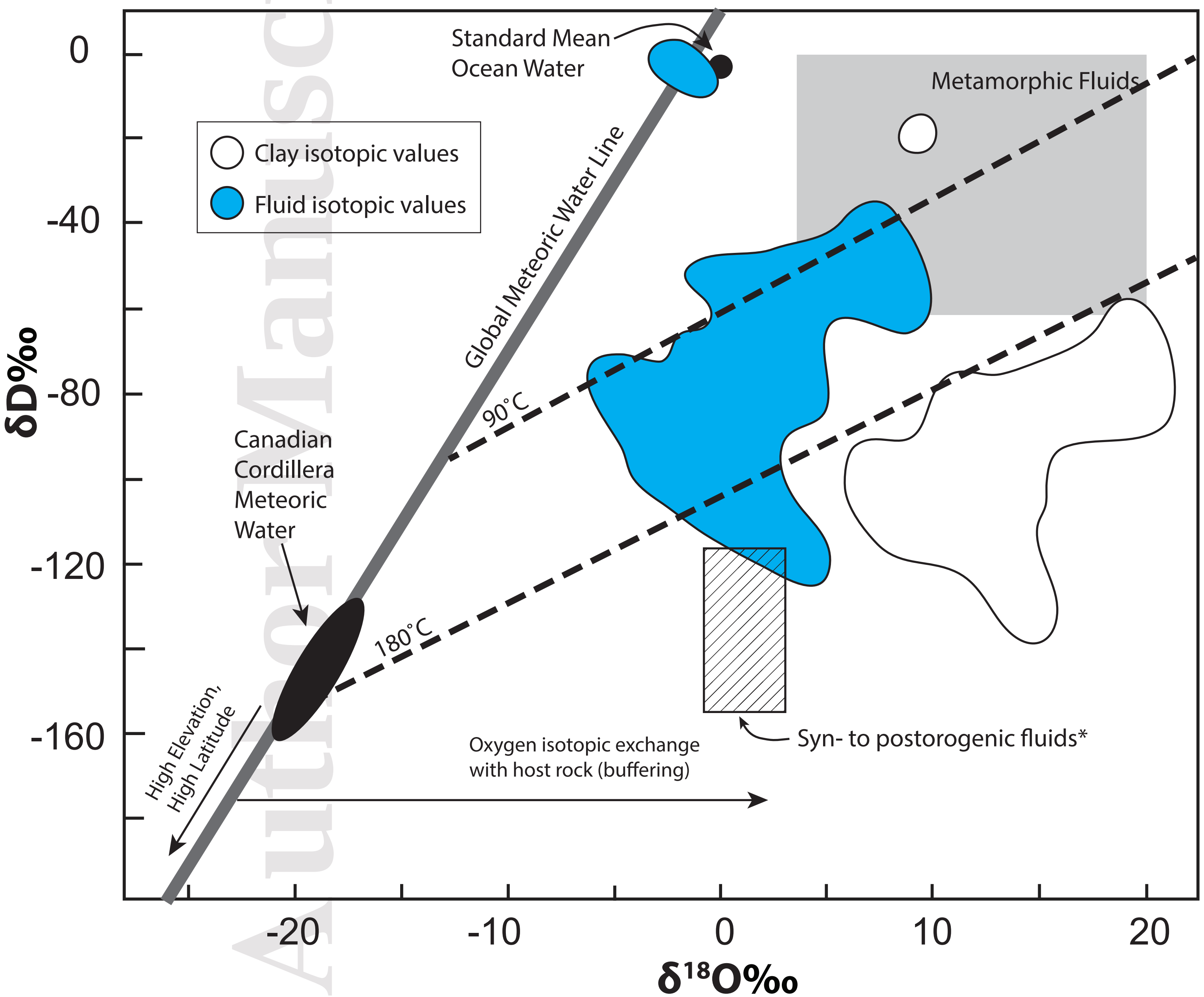

Standard Mean
Ocean Water
Metamorphic Fluids
Clay isotopic values
Fluid isotopic values
Global Meteoric Water Line
90°C
180°C
Canadian
Cordillera
Meteoric
Water
High Elevation,
High Latitude
Oxygen isotopic exchange
with host rock (buffering)
Syn- to postorogenic fluids*
0
-40
-80
-120
-160
δD‰
-20
-10
0
10
20
δ18O‰

Table 1. Sample Locations and Descriptions

Sample ID	Fault	Hanging Wall	Foot Wall	Latitude	Longitude
1. DP10-406C	Muskeg Thrust	Gates sandstone *Lower Cretaceous*	Kaskapau shale/siltstone *Upper Cretaceous*	54° 1' 21.0" N	119° 3' 36.7" W
2. DP11-90	Broadview (Snake Indian) Thrust	Whitehorse silty dolomite *Triassic*	Fernie shale *Jurassic*	53° 48' 47.7" N	119° 44' 48.7" W
3. DP11-100	Rocky Pass Thrust	Rundle carbonate *Mississippian*	Nikanassin shale/siltstone *U.Jurassic – L.Cretaceous*	53° 37' 22.9" N	118° 52' 18.7" W
4. DP10-166D	Brule Thrust	Palliser carbonate *Upper Devonian*	Nikanassin shale/siltstone *U.Jurassic – L.Cretaceous*	53° 16' 49.8" N	117° 53' 21.8" W
5. DP10-140A	Greenock Thrust	Lower Rundle carbonate *Mississippian*	Fernie shale *Jurassic*	53° 3' 14.0" N	117° 58' 4.1" W
6. DP10-11	Nikanassin Thrust	Palliser carbonate *Upper Devonian*	Nikanassin shale/siltstone *U.Jurassic – L.Cretaceous*	53° 0' 16.3" N	117° 18' 47.4" W
7. DP10-1	Pyramid Thrust (Jasper)	Miette grit *Neoproterozoic*	Perdix/Sassenach shale *Upper Devonian*	52° 55' 4.8" N	118° 3' 11.9" W
8. DP11-104	Sulphur Mt. Thrust (Abraham Lake)	Rundle carbonate *Mississippian*	Fernie shale *Jurassic*	52° 16' 36.8" N	116° 34' 58.4" W
9. DP10-2	McConnell Thrust (Abraham Lake)	Eldon carbonate *Middle Cambrian*	Luscar shale/siltstone *Lower Cretaceous*	52° 16' 10.7" N	116° 23' 35.7" W
10. DP11-107	Johnston Creek Thrust	Miette sand/siltstone, grit *Neoproterozoic*	Eldon carbonate *Middle Cambrian*	52° 3' 9.2" N	116° 30' 16.7" W
11. DP11-114	Clearwater Thrust	Banff carbonate *Mississippian*	Kootenay shale/siltstone *U.Jurassic – L.Cretaceous*	52° 3' 19.1" N	116° 4' 31.1" W
12. DP11-112	Simpson Pass Thrust	Gog qtzite/qtz sandstone *Lower Cambrian*	Pika carbonate *Middle Cambrian*	51° 41' 35.6" N	116° 25' 10.9" W
16. KKF-91-1A	Sulphur Mt. Thrust (Kananaskis)	Palliser carbonate *U. Devonian*	Fernie shale *Jurassic*	50° 53' 59.8" N	114° 56' 33.8" W
18. KKF-102E	Lewis Thrust	Palliser carbonate	Belly River shale/siltstone	50° 2' 6.9" N	114° 38' 42.5" W

18. KRF-102E	(Gould Dome)	*U. Devonian*	*Upper Cretaceous*	50° 2' 6.9" N	114° 58' 42.5" W
A. MTF-FW2	McConnell Footwall shale sample	--	Luscar shale/siltstone *Lower Cretaceous*	52° 16' 10.7" N	116° 23' 35.7" W

Table 2. *Mineralogy of Samples*

		MRI Quantification			Illite Polytype*	
Sample ID	Size Fraction	%Chl	%Kaol	%Ill	%$2M_1$	%$1M_d$
1. DP10-406C	C	-	37	63	21	79
Muskeg Thrust	MC	-	23	77	16	84
	M	-	4	96	10	90
	F	-	-	100	6	94
2. DP11-90	C	-	10	90	19	81
Broadview (Snake Indian) Thrust	MC	-	5	95	14	86
	M	-	-	100	9	91
	F	-	-	100	5	95
3. DP11-100	C	-	-	100	36	64
Rocky Pass Thrust	MC	-	-	100	26	74
	M	-	-	100	17	83
	F	-	-	100	13	87
4. DP10-166D	C	-	-	100	24	76
Brule Thrust	MC	-	-	100	18	82
	M	-	-	100	11	89
	F	-	-	100	6	94
5. DP10-140A	C	-	-	100	32	68
Greenock Thrust	MC	-	-	100	30	70
	M	-	-	100	9	91
	F	-	-	100	2	98
6. DP10-11	C**	?	?	?	38	62
Nikanassin Thrust	MC***	?	?	?	19	81
	M	-	-	100	11	89
	F	-	-	100	6	94
7. DP10-1	C	-	-	100	28	72
Pyramid Thrust (Jasper)	M	-	-	100	16	84
	F	-	-	100	11	89
8. DP11-104	C	23	-	77	42	58
Sulphur Mt. Thrust (Abraham Lake)	MC	17	-	83	29	71
	M	5	-	95	11	89
	F	-	-	100	7	93

9. DP10-2	C	-	-	100	20	80
McConnell Thrust (Abraham Lake)	MC	-	-	100	16	84
	M	-	-	100	8	92
	F	-	-	100	6	94
10. DP11-107	C	29	-	71	41	59
Johnston Creek Thrust	MC	24	-	76	31	69
	M	14	-	86	22	78
	F	18	-	82	11	89
11. DP11-114	C	-	-	100	32	68
Clearwater Thrust	MC	-	-	100	18	82
	M	-	-	100	11	89
	F	-	-	100	8	92
12. DP11-112	C	12	-	88	52	48
Simpson Pass Thrust	MC	7	-	93	33	67
	M	6	-	94	11	89
	F	-	-	100	7	93
16.KKF-91-1A						
Sulphur Mt. Thrust (Kananaskis)	C	-	-	100	30	70
	M	-	-	100	5	95
	F	-	-	100	5	95
18. KKF-102E	C	-	57	43	73	27
Lewis Thrust (Gould Dome)	M	-	30	70	39	61
	F	-	5	95	18	82
A. MTF-FW2	C	-	-	100	32	68
McConnell Footwall Shale	M	-	-	100	8	92
	F	-	-	100	6	94

* From Pană & van der Pluijm (2015)

**No oriented sample available

***Clay minerals not identifiable in oriented samples

(tr) - trace

%1M_d/clay	non-clay minerals
50	qtz
35	qtz
14	qtz
6	-
27	qtz
18	?
9	cct
5	cct
36	qtz, cct
26	cct
17	cct
13	cct
24	qtz
18	qtz
11	-
6	-
68	qtz
70	qtz(tr)
91	-
98	-
62**	?
81***	?
89	-
94	-
7	qtz
84	qtz
89	qtz, gyp
55	qtz, cct
41	qtz, cct
15	cct
7	cct(tr)

80	qtz
84	qtz
92	-
94	-
58	qtz
48	qtz
33	cct
27	cct
68	qtz
82	qtz
89	-
92	-
58	qtz
38	-
16	-
7	cct
70	qtz
95	-
95	-
12	qtz
43	-
78	-
68	qtz
92	-
94	-

Table 3. *Hydrogen Isotopic Results*

Sample ID	Size Fraction	δD (‰)	dupl. (‰)	Sample ID	Size Fraction	δD (‰)
1. DP10-406C	C	-83.5	-84.1	**8. DP11-104**	C	-101.7
Muskeg Thrust	MC	-74.6	-75.6	*Sulphur Mt. Thrust (Abraham Lake)*	MC	-100.1
	M	-94.4	-96.4		M	-86.8
	F	-101.9	-101		F	-73.8
2. DP11-90	C	-71.1	-72.7	**9. DP10-2**	C	-110.7
Broadview (Snake Indian) Thrust	MC	-69.2	-71.1	*McConnell Thrust (Abraham Lake)*	MC	-107.6
	M	-64	-65.6		M	-92.5
	F	-66.4	-65.8		F	-89.4
3. DP11-100	C	-121.4	120.5	**10. DP11-107**	C	-80.4
Rocky Pass Thrust	MC	-118.8	-118.3	*Johnston Creek Thrust*	MC	-95
	M	-102	-101.6		M	-97.2
	F	-95.8	-97		F	-89.5
4. DP10-166D	C	-73.6	-73.9	**11. DP11-114**	C	-116.8
Brule Thrust	MC	-98.8	-98.1	*Clearwater Thrust*	MC	-125.9
	M	-97.3	-97.4		M	-118.9
	F*	-42.6	-44.6		F	-108
5. DP10-140A	C	-94.2	-95	**12. DP11-112**	C	-115.5
Greenock Thrust	MC	-98.2	-95.6	*Simpson Pass Thrust*	MC	-112.9
	M	-102.6	-102.4		M	-120.4
	F	-78.4	-78.5		F	-98.2
6. DP10-11	C	-112.2	-114.7	**16. KKF-91-1A**		
Nikanassin Thrust	MC	-114.9	-115.1	*Sulphur Mt. Thrust (Kananaskis)*	C	-119.1
	M	-104.4	-103.9		M	-106.5
	F	-107	-103.9		F	-116.3
7. DP10-1	C	-105.7	-105.5	**18. KKF-102E**	C	-127.9
Pyramid Thrust (Jasper)	M	-81.9	-81.8	*Lewis Thrust (Gould Dome)*	M	-124.3
	F	-49.2	-51.1		F	-115.9
				A. MTF-FW2	C	-117.2
			*Organic-rich sample	*McConnell Footwall Shale*	M	-95.2
					F	-102.7

dupl. (‰)
-101.7
-100.3
-86.9
-73.9
-111.8
-110.8
-90.6
-87.6
-79.5
-94.8
-96.4
-89
-118.2
-125
-116.6
-108.3
-114.1
-115
-116.7
-96
-120.4
-107.1
-116.1
-129.8
-124
-114.1
-118.5
-95.4
-100.8

Table 4. *Isotopic Composition of Authigenic Illite*

Sample ID	Fault/Description	$\delta D_{authigenic}$	δO_{fine} (±2‰)
1. DP10-406C	Muskeg Thrust	-105.7 ± 2.9‰	12.0‰
2. DP11-90	Broadview (Snake Indian) Thrust	-63.1 ± 2.0‰	19.3‰
3. DP11-100	Rocky Pass Thrust	-80.8 ± 6.8‰	20.3‰
4. DP10-166D	Brule Thrust	35.4 ± 72.1‰* -136.5 ± 22.4‰**	14.6‰
5. DP10-140A	Greenock Thrust	-71.9 ± 7.3‰	17.1‰
6. DP10-11	Nikanassin Thrust	-102.1 ± 2.3‰	14.6‰
7. DP10-1	Pyramid Thrust (Jasper)	-17.8 ± 19.9‰	9.4‰
8. DP11-104	Sulphur Mt. Thrust (Abraham Lake)	-73.1 ± 2.4‰	16.5‰
9. DP10-2	McConnell Thrust (Abraham Lake)	-77.3 ± 8.1‰	11.4‰
10. DP11-107	Johnston Creek Thrust	-117.6 ± 8.6‰	11.6‰
11. DP11-114	Clearwater Thrust	-96.5 ± 11.7‰	10.7‰
12. DP11-112	Simpson Pass Thrust	-96.9 ± 4.3‰	7.0‰
16. KKF-91-1A	Sulphur Mt. Thrust (Kananaskis)	-107.7 ± 2.5‰	--
18. KKF-102E	Lewis Thrust (Gould Dome)	-110.8 ± 2.1‰	8.3‰, 8.1‰***
A. MTF-FW2	McConnell Footwall Shale	-92.1 ± 3.3‰	13.5‰, 13.3‰***

*Using all size fractions

**Without fine fraction

***Duplicate

Table 5. *Isotopic Composition of Fault Fluids*

	Hydrogen (δD‰)		Oxygen (δ^{18}O‰)	
Sample ID	90°C (min)	180°C (max)	90°C	180°C
1. DP10-406C	-76	-101	-2.4	4.1
2. DP11-90	-33	-58	4.9	11.4
3. DP11-100	-51	-76	6	12.4
4. DP10-166D	-106	-131	0.2	6.7
5. DP10-140A	-42	-67	2.7	9.2
6. DP10-11	-72	-97	0.2	6.7
7. DP10-1*	12	-13	-5	1.5
8. DP11-104	-43	-68	2.2	8.6
9. DP10-2	-47	-72	-3	3.5
10. DP11-107	-88	-112	-2.8	3.7
11. DP11-114	-66	-91	-3.7	2.8
12. DP11-112	-67	-92	-7.4	-0.9
16. KKF-91-1A	-78	-102	-	-
18. KKF-102E	-81	-106	-6.1, -6.3	0.4, 0.2
A. MTF-FW2	-63	-88	-0.9, -1.1	5.6, 5.4
Average	-66	-90	-1.2	5.3
	-78 ± 13		2.1 ± 3.3	
Minimum	-106	-131	-7.4	-0.9
	-119 ± 13		-4.2 ± 3.3	
Maximum	-33	-58	6	12.4
	-46 ± 13		9.2 ± 3.3	

*Outlier: not included in Average, Minimum, and Maximum